

pubs.acs.org/acscatalysis Research Article

Counting Sites in Lewis Acid Zeolite Sn-Beta: Connecting Site Quantification Experiments and Spectroscopy To Investigate the Catalytic Activity for the Alcohol Ring Opening of Epoxides

Leah Ford, Alexander Spanos, and Nicholas A. Brunelli*



Cite This: ACS Catal. 2023, 13, 11422–11432



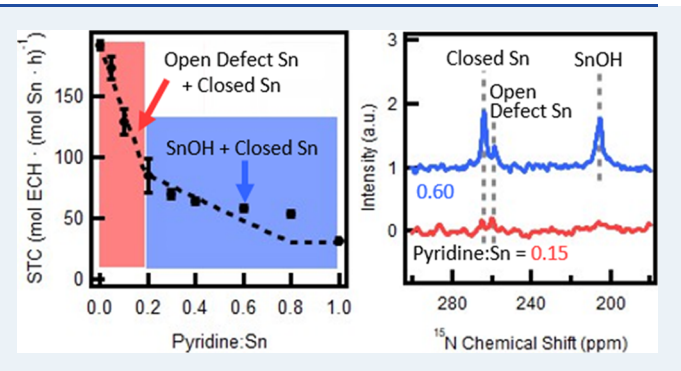
ACCESS I

Metrics & More

Article Recommendations

Supporting Information

ABSTRACT: Sn-Beta is a promising catalyst for numerous reactions involved in biomass upgrading and fine chemical production, but it is complex with multiple types of active sites. The activity for Sn-Beta can be calculated on a per-site basis using site quantification experiments that involve adding a Lewis basic probe molecule, but it is not clear which types of sites are being titrated. Our work connects site quantification experiments with spectroscopic measurements to explain differences in the catalytic activity of materials crystallized for different amounts of time. For alcohol ring opening of epoxides, experiments reveal that Sn-Beta crystallized for 10 days (Sn-Beta-200-10d) is more active than Sn-Beta crystallized for 40 days (Sn-Beta-200-40d). These materials



are investigated using site quantification experiments with three probes—triethylamine, pyridine, or 2,6-lutidine—to reveal the different fractions and types of sites. As the probe:Sn ratio is increased, these experiments result in two distinct slopes, indicating two distinct activities: high and low activity. The difference in activity between Sn-Beta-200-10d and Sn-Beta-200-40d can be attributed to the reduced fraction of high-activity sites. Although the two slopes have typically been assigned to open defect Sn sites for high activity and closed Sn sites for low activity, ¹⁵N NMR measurements of materials dosed with ¹⁵N-labeled pyridine contradict this assignment. Indeed, at low concentrations, pyridine adsorbs on both open defect and closed Sn sites whereas the low activity corresponds to pyridine binding to SnOH groups in addition to closed Sn sites. Overall, the identification of appropriate site quantification experiment parameters and the combination of these titrations with NMR techniques allows for the establishment of a synthesis—structure—activity relationship that has the potential to improve the performance of Sn-Beta.

KEYWORDS: Sn-Beta, epoxide ring opening, site quantification, Lewis acid zeolite, NMR, pyridine

1. INTRODUCTION

Interest in Lewis acid zeolites has exploded with the discovery of synthetic methods to produce highly crystalline, pure silica materials containing heteroatoms such as Sn, Zr, and Hf. --These materials can catalyze many important and exciting reactions, 4-26 adding a new dimension to our current catalytic capabilities. Yet, these materials were quickly discovered to be rather complex, containing multiple types of catalytic sites. The different types of sites have been demonstrated through complementary forms of spectroscopy and are often correlated with the catalyst activity, with each site having a different activity for a given reaction. Other site quantification experiments have been used to reveal distinct activity levels that are consistent with the catalyst having multiple types of sites, but the nature of these sites has not been rigorously identified. Additional research is necessary to establish the connection between the spectroscopic structure of the sites and the activity of the catalyst.

Lewis acid zeolites may be promising for improving the efficiency of important industrial reactions, but their

nonuniformity poses a challenge as researchers attempt to elucidate their synthesis—structure—activity relationships. One such complex zeolite is Sn-Beta, which has been proposed to have different catalytic sites, including (a) "closed" sites, (b) "hydrolyzed-open" sites, and (c) "open defect" sites (Figure 1).²⁷ Closed sites are comprised of a tin atom tetrahedrally coordinated through four siloxane bonds. When closed sites hydrolyze at the oxygen bridge between the tin and silicon, they form hydrolyzed-open sites, which can then transform back to closed sites upon dehydration. Lastly, open defect tin sites are adjacent to a missing framework silicon atom.²⁷ These structural distinctions are important because it is expected that

Received: June 7, 2023 Revised: July 21, 2023 Published: August 15, 2023





(a)
$$H_{20}$$
 (b) (c) H_{20} H_{20}

Figure 1. Catalytic sites in Sn-Beta, specifically (a) closed, (b) hydrolyzed-open, and (c) open defect sites.

open sites have different binding energy than closed sites, ²⁸ causing different activities for specific reactions; there is evidence that open defect sites are more active for glucose isomerization, ^{28–33} MPVO, ^{34,35} Baeyer–Villiger oxidation, ^{34,36} and epoxide ring opening (ERO), ¹⁹ whereas closed sites are correlated to the activity for ethanol dehydration ^{33,37} and aldol condensation. ^{38,39} As different sites exist, it is important to accurately quantify the catalytic site distribution to establish synthesis–structure–activity relationships for Sn-Beta.

This philosophy was exemplified by Kolyagin et al. as they studied the effect of crystallization time on Sn-Beta activity for MPVO reactions. ¹⁰ Interestingly, it was discovered that Sn-Beta activity for MPVO conversion of cyclohexanone was maximized at a crystallization time of approximately 13 days, beyond which performance was significantly reduced. Materials were characterized via NMR for site quantification to attribute the lower activity to a decrease in high-activity "group I" and "group 2" sites, but the measurements do not establish the nature of the site or the activity on a per-site basis. As synthesis—structure—activity relationships continue to be developed, catalytic site quantification will be crucial for establishing structure—activity connections, which are currently limited.

Commonly reported methods to characterize the types of catalytic sites in Sn-Beta include infrared spectroscopy (IR)²⁷ and nuclear magnetic resonance spectroscopy (NMR).40 One standard IR technique is diffuse reflectance Fourier transform infrared spectroscopy (DRIFTS) wherein a Lewis base probe molecule—typically deuterated acetonitrile (CD₃CN)—is adsorbed to the Lewis acid sites prior to the collection of spectra. 20,28,29,41-43 It is expected that CD₃CN adsorption on a Lewis acid weakens the C≡N bond proportionally to the Lewis acid strength; the interaction causes IR peaks to shift away from that of uncoordinated CD₃CN. FTIR with CD₃CN has shown to be effective at differentiating Lewis acid sites with varying acid strengths. 44-47 Specifically, it has been proposed that peaks at 2316 and 2308 cm⁻¹ correspond to CD₃CN adsorbed to open and closed sites, respectively.³⁶ Despite the widespread use of DRIFTS as a site quantification technique, an incomplete understanding of the interactions between the acetonitrile molecules and catalytic sites has caused some

researchers to question the assignment of specific peak shifts with different types of sites. 48

Unlike DRIFTS, ¹¹⁹Sn NMR can be a direct and quantitative method to determine the active site coordination and identity of Sn in Sn-Beta materials without the use of probe molecules. ^{17,40,49–52} However, the low natural abundance of the ¹¹⁹Sn isotope (8.59%) coupled with the low Sn incorporation in the materials (0.5–1%) makes ¹¹⁹Sn NMR challenging without long analysis times or expensive, isotopically enriched materials. Despite the development of strategies to overcome these challenges, such as using advanced Dynamic Nuclear Polarization NMR techniques, ^{10,53,54} recent investigations have focused on alternative NMR methods for site quantification involving the use of Lewis basic probe molecules. ⁵⁵

The challenges associated with ¹¹⁹Sn NMR can be overcome through analysis with ³¹P NMR following the adsorption of Lewis basic phosphorus-containing probe molecules to Sn-Beta materials. As the NMR active ³¹P nucleus is 100% naturally abundant, this analysis has improved sensitivity as compared to ¹¹⁹Sn NMR. Recent work to establish ³¹P NMR as a viable characterization technique has identified trimethylphosphine oxide (TMPO) as a probe molecule that is able to differentiate types of Lewis-acidic sites. 55-59 Specifically, following the addition of TMPO in dichloromethane (DCM), peaks located at \sim 55 and \sim 58 ppm are believed to be associated with unique Sn framework sites in Sn-Beta. 17,35,38 Probe molecule interactions are under investigation to corroborate NMR peak assignments to specific catalytic site structures or coordination environments. 60,61 Although 31P NMR appears promising for site quantification, the use of TMPO may limit comparison to other site quantification techniques, as TMPO has limited solubility in solvents except for DCM, which may be problematic since the solvent can impact the site quantification experiments.43

To improve the potential for connecting NMR spectroscopy to other site quantification techniques, ¹⁵N MAS NMR may be performed using ¹⁵N-labeled pyridine as a probe molecule. Pyridine can be dosed to the catalyst in hexane, a solvent that we have used previously for site quantification techniques. ⁴³ ¹⁵N NMR using pyridine has been shown to produce peaks at 260 and 265 ppm (referenced to liquid ammonia) for Sn-Beta, representing Sn sites with different Lewis acidity. ⁶² Overall, spectroscopic techniques such as FTIR and NMR are valuable for site characterization, but they do not provide direct insight into the catalytic contributions of different sites, spurring investigation into techniques that allow for site quantification in tandem with catalytic testing.

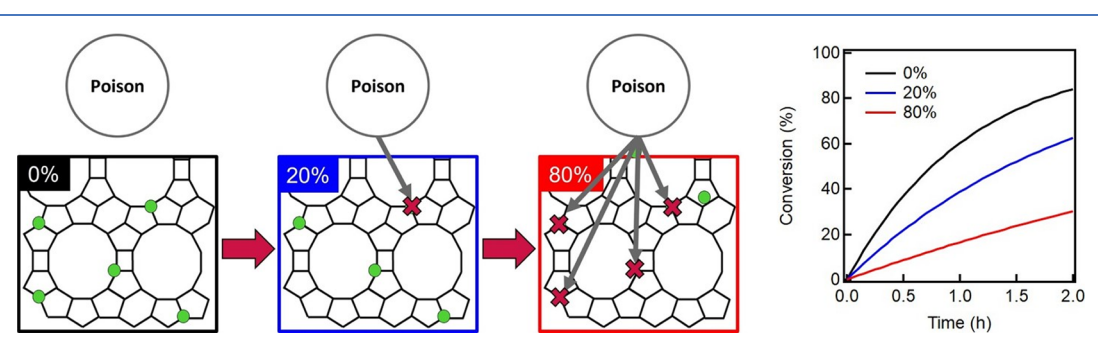


Figure 2. Schematic of site quantification experiments, in which a probe molecule is added to the catalyst in increasing amounts to deactivate and thereby quantify active sites.

Site quantification experiments involve the addition of Lewis basic probe molecules to deactivate a certain fraction of the Sn sites prior to catalyzing the reaction (Figure 2). The ratio of the probe molecule to catalytic sites is increased until no conversion is observed, at which point all active sites are believed to have been deactivated. The current understanding is that some Lewis base probes adsorb preferentially to catalytic sites with high Lewis acid strength, allowing for the differentiation of sites with distinct structures.

Site quantification experiments have been applied to zeolite Beta, ^{28,33,43} other zeolite frameworks, ³³ and mesoporous catalysts such as amine-functionalized SBA-15. ^{63–65} For Sn-Beta, Harris et al. used pyridine for titration experiments and complemented these results with FTIR using acetonitrile to identify open defect sites as the dominant sites for glucose isomerization, ²⁸ corroborating earlier findings. ^{4,29} Bates et al. later expanded upon this work and determined that closed Sn sites were more active than open defect Sn sites for ethanol dehydration using similar techniques. ³³

Overall, site quantification experiments are a promising technique with the ability to quantify distinct catalytic sites and their respective activities, causing them to be conducted more frequently in zeolite research. However, several challenges remain in that there is (1) limited investigation of experimental parameters and (2) limited understanding of how poisoning occurs on a molecular level. In this work, we address these challenges by (a) investigating the impact of selected poison on site quantification experiment results and (b) establishing a connection between site quantification experiments and results from spectroscopic techniques.

The selection of an appropriate probe is necessary for accurate quantification of catalytic sites. Ideally, a probe should have minimal catalytic activity for the given reaction at the test conditions, a size or flexibility that allows it to travel through the catalyst pores to deactivate sites without diffusion limitations, and preferential adsorption that enables the differentiation of catalytic sites with varying activity levels. Previous work in our group has used triethylamine (TEA) as a probe molecule for zeolite Sn-Beta. 43 Other commonly employed Lewis basic titrants include pyridine^{28,62,66} and 2,6-lutidine. 67-71 Pyridine has previously been used in site quantification experiments to distinguish catalytic sites through the titration of Sn-Beta sites and subsequent assessment of catalytic activity for ethanol dehydration and glucose isomerization.³³ 2,6-lutidine has been shown to distinguish Brønsted acid sites in zeolites, but not Lewis acid sites. 67-69 Although these molecules have each been used as probe molecules, a direct comparison has not yet been presented. Furthermore, when considering the selection of a probe for site quantification, the molecule should be NMR active such that NMR measurements may inform the structures of titrated sites.

Here, we investigate three Lewis bases—TEA, pyridine, and 2,6-lutidine—as potential probes for site quantification experiments, as they have each demonstrated promise as site titrants and can be isotopically enriched for NMR analysis. Each base is investigated to assess the occurrence of diffusion limitations within the Sn-Beta materials by varying the length of time for which the probe molecule and catalyst are stirred before beginning catalytic testing for the ERO of epichlorohydrin (ECH) by methanol (Figure 3). The data gathered by site quantification experiments using each probe are compared in terms of the calculated percentage of active sites and the differentiation (or lack thereof) of structurally different

Figure 3. Reaction scheme for ERO of epichlorohydrin by methanol.

catalytic sites. Upon determination of an appropriate probe molecule, the distribution of catalytic sites in Sn-Beta is investigated as a function of crystallization time. Furthermore, this work aims to better understand the results of site quantification experiments using ¹⁵N NMR spectroscopy. Importantly, the ¹⁵N NMR measurements enable observation of the types of sites that are titrated. Sn-Beta materials are characterized using each of these techniques, and results are used to determine catalytic site distributions as well as the catalytic contributions from the different types of sites.

2. EXPERIMENTAL METHODS

2.1. Sn-Beta Synthesis and Characterization. Conventional Sn-Beta-200 is synthesized hydrothermally following a previously reported procedure. Two batches of materials are synthesized with different crystallization times of 10 and 40 days. Synthesis details and chemical information can be found in the Supplemental Information (SI).

The synthesized materials are characterized using numerous standard techniques, including powder X-ray diffraction (PXRD), nitrogen physisorption, water adsorption, elemental analysis using inductively coupled plasma optical emission spectroscopy (ICP-OES), diffuse reflectance ultra-violet visible spectroscopy (DRUVS), DRIFTS, and scanning electron microscopy (SEM). Characterization procedural details can be found in the SI.

2.2. Catalytic Testing for Epoxide Ring Opening. Similar to our previous work, 19,20,43 the materials are tested for catalytic activity for ERO between epichlorohydrin and methanol in a 10-mL two-neck round-bottom (RB) flask with a condenser attached to the straight neck and a septum covering the slant neck. ECH (0.4 M) in methanol (2 mL) is added to the RB along with 1,3,5-trimethoxybenzene (TMB; 0.06 M) as an internal standard. After 2 min of mixing (600 RPM), two t_0 samples (40 μ L) are taken and diluted with acetone. The catalyst is added to the reaction mixture with the quantity of catalyst used being the mass required to achieve an ECH:Sn of 250:1. The RB is immersed in a silicone oil bath preheated to 60 °C using a Heidolph stir plate. It has previously been demonstrated that the reactants do not experience significant internal mass transfer limitations through Sn-Beta at these reaction conditions.⁴³

At specific times (15 min, 30 min, 1 h, 1.5 h, and 2 h), a sample (40 μ L) is drawn through the septum using a reusable stainless-steel needle, filtered through a silica/cotton plug, and diluted with acetone. All samples are analyzed using an Agilent 7820A gas chromatograph equipped with a flame ionization detector (GC-FID). The two t_0 samples are averaged to determine initial epichlorohydrin concentrations. Using the initial concentrations, conversion is computed using the TMB internal standard as a basis. Tests are repeated between 2 and 4 times each, and data are reported as average values with calculated standard deviations.

2.3. Site Quantification Experiments. The ERO reaction between epichlorohydrin and methanol is conducted in a 10-mL two-neck RB flask with a condenser attached to the straight neck and a septum covering the slant neck. The desired catalyst is added to the RB, then a specific ratio of

probe:Sn sites is achieved using a solution containing the probe in hexane (0.5 mL). The probes tested are TEA, pyridine, and 2,6-lutidine. Upon addition of the probecontaining solution, the contents of the RB are stirred for Δt = 2 min (600 RPM) at ambient temperature before adding the well-stirred reaction mixture (1.5 mL), which consists of ECH (0.4 M) and TMB (0.06 M) in methanol. The initial ECH:Sn is 250:1. Two t_0 samples (40 μ L) are taken directly from the reaction mixture and diluted with acetone before adding the mixture to the RB. The RB is immersed in a silicone oil bath preheated to 60 °C using a Heidolph stir plate with a stirring rate of 600 RPM. Sample collection and analysis follow the same procedure as described in Section 2.2.

2.4. ¹⁵N MAS NMR Spectroscopy. ¹⁵N MAS NMR is conducted in a 600 MHz (1H) Bruker Avance III HD spectrometer using a 3.2 mm HXY DNP probe tuned in double mode to ¹H/¹⁵N. Approximately 150 mg of Sn-Beta is re-calcined at 550 °C for 10 h and degassed under vacuum (~20 millitorr) at 140 $^{\circ}\text{C}$ overnight. In a glovebox under inert conditions, the Sn-Beta is wetted with ~1 mL of hexane, then a solution of ¹⁵N-labeled pyridine in hexane is added to the material to achieve pyridine:Sn values of 0.15:1, 0.3:1, and 0.6:1, and the mixtures are stirred overnight (350 RPM) at ambient temperature. Hexane is removed by heating the mixture to 120 °C in an oil bath under vacuum (~100 millitorr) overnight. The final material to which pyridine has been added is packed into the rotor in a glovebox under inert conditions. The sample is spun at 15 kHz MAS and analyzed for ¹⁵N nuclei using CPMAS with 90 kHz ¹H decoupling, 64,000 scans, and a 2.5 s recycle delay. The data are referenced externally to ammonium chloride.

3. RESULTS AND DISCUSSION

3.1. Characterization of Sn-Beta-200 Materials. Sn-Beta-200-10d and Sn-Beta-200-40d (Sn-Beta-x-y; $x = \frac{1}{2}$ theoretical Si:Sn and y = crystallization time) are hydrothermally synthesized in fluoride media and characterized using standard techniques, including PXRD, nitrogen physisorption, water adsorption, elemental analysis, DRUVS, DRIFTS, and SEM. PXRD patterns of both materials are consistent with *BEA patterns obtained from the International Zeolite Association database, indicating the successful synthesis of zeolite Beta (Figure S1). Nitrogen adsorption curves show that the materials uptake high quantities of nitrogen at low relative pressures (0-0.01) and then plateau at higher relative pressures, consistent with microporous behavior (Figure S2). Calculated t-plot micropore volumes are 0.20 cm³/g, which is comparable to previous values for highly crystalline zeolite Beta (Table 1).^{1,8} Water adsorption results indicate that at 0.2 relative pressure, Sn-Beta-200-40d adsorbs 6.9 cm³ water/g STP and Sn-Beta-200-10d adsorbs 8.4 cm³ water/g STP (Figure S3). Compared to the amount of water adsorption at 0.2 relative pressure for hydrophobic Si-Beta-F

Table 1. Characterization Results for Sn-Beta Materials

sample	BET surface area $(m^2/g)^a$	t-plot micropore volume $(cm^3/g)^a$	theoretical Si:Sn	actual Si:Sn ^b
Sn-Beta-200-10d	589 ± 0.7	0.20	200	191
Sn-Beta-200-40d	604 ± 0.7	0.20	200	222

^aCalculated from nitrogen physisorption isotherms. ^bDetermined from elemental analysis using ICP-OES.

(F-mediated pure silica Beta; 1.3 cm³/g STP) and hydrophilic de-Al-Beta-OH (dealuminated zeolite Beta made using hydroxide mediated conditions; 73 cm³/g STP), Sn-Beta-200-10d and Sn-Beta-200-40d are considered to have similar hydrophobicity. Elemental analysis is performed using ICP-OES, and actual Si:Sn values are determined to be 191 and 222 for the 10 and 40 day samples, respectively (Table 1).

DRUVS results suggest the presence of isolated Sn sites and limited to no SnO₂ in both Sn-Beta materials (Figure S4), consistent with previously synthesized Sn-Beta materials.¹⁷ A small difference in intensity of the peak at ~210 nm is observed, but the difference has been observed for a single sample when analyzing the same sample multiple times and reflects the complexity of interpreting UV spectra for metal oxide materials. Overall, the DRUVS results are sufficiently similar for Sn-Beta-200-10d and Sn-Beta-200-40d that it is not expected that any differences in activity would be attributed to differences regarding the amount of inactive SnO₂ nanoparticles formed during hydrothermal synthesis, as opposed to SnO₂ clusters formed during post-synthetic insertion that are reported to be active.¹⁷ DRIFTS is performed by collecting spectra after dosing increasing quantities of CD₃CN to Sn-Beta-200-10d and Sn-Beta-200-40d. Specifically, peaks in the spectrum have been assigned to CD₃CN adsorbed to open defect Sn sites (2316 cm⁻¹), closed Sn sites (2307 cm⁻¹), and silanols (2278 cm⁻¹), and physisorbed CD₃CN (2268 cm⁻¹). Spectra for both materials exhibit peaks at these locations (Figure S5), indicating the presence of different types of Sn sites as well as silanols.

SEM images show that Sn-Beta-200-10d and Sn-Beta-200-40 have comparable particle sizes, with most of the particles having sizes from approximately 3 to 5 μ m (Figure S6). Therefore, any differences in catalytic activity are likely not attributed to differences in particle size and subsequent diffusion limitations.

Overall, these results indicate the successful synthesis of Sn-Beta-200-10d and Sn-Beta-200-40d materials with characteristics that are consistent with previous syntheses. Furthermore, standard characterization results of these materials are comparable, making it easier to directly compare their catalytic activities and catalytic site distributions.

3.2. Catalytic Performance for Epoxide Ring Opening. Sn-Beta-200-10d and Sn-Beta-200-40d are tested for catalytic activity for ERO between ECH and methanol. As shown in Figure 4, the GC-FID data from analyzed samples are converted to conversion over time. It is observed that both materials display high catalytic performance for this reaction at these conditions, consistent with previous work. 19,20 Sn-Beta-200-10d exhibits a higher catalytic activity for this reaction as compared to Sn-Beta-200-40d, with the two materials achieving conversions at 2 h of 95 and 90%, respectively. The data are fit using a first-order exponential model and then normalized by the initial molar quantity of ECH and total molar quantity of Sn to calculate site time conversion (STC). The values of STC for Sn-Beta-200-10d and Sn-Beta-200-40d are determined to be 393 ± 16 and $295 \pm 35 \text{ h}^{-1}$, respectively, indicating a lower activity for the material with a longer crystallization time.

As determined through standard characterization, the difference in activity is not explained by differences in crystallinity, microporosity, or differences in SnO_2 nanoparticle formation. Additionally, the difference in hydrophobicity of Sn-Beta-200-40d does not explain the difference in activity, as

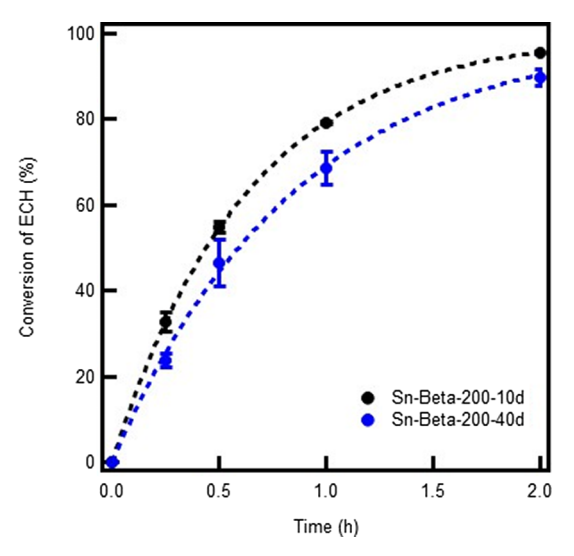


Figure 4. Comparison of catalytic performance of Sn-Beta-200-10d and Sn-Beta-200-40d for the conversion of ECH with methanol. The amount of each catalyst gives a constant ECH:Sn of 250:1. The error bars indicate one standard deviation. The reaction is performed using 0.4 M epichlorohydrin and 0.06 M TMB (internal standard) in 2 mL methanol at 60 $^{\circ}\text{C}$ and 600 RPM. The selectivity for the terminal ether is determined to be constant at 97% for the different materials at each time point.

previous results suggest that increased hydrophobicity actually improves performance for ERO (Figure S3).⁴³

These results are reminiscent of other studies in which activity for a given reaction changes with crystallization time. Decifically, it has been shown that activity for MPVO is maximized at a Sn-Beta crystallization time of 13 days, and the activity decreases for materials synthesized using longer crystallization times. Noting these similar trends and recalling that the open defect site is proposed to be the dominant active site for both MPVO Add and ERO, and ERO, is possible that changes in activity are associated with differences in the fraction of different sites in the materials. We investigate the potential impact of catalytic site distributions on ERO activity for the materials crystallized for different lengths of time using site quantification experiments.

3.3. Site Quantification Experiments on Sn-Beta-200-10d. The site quantification experiments are performed using hexane as the solvent since our previous work has shown that hexane does not interact with the catalytic sites or impact site quantification results because it is nonpolar. Following the addition of the probe solution, ERO between ECH and methanol is conducted, and STC is calculated. This process is repeated at increasing quantities of probe molecule up to a probe: Sn value of 1:1. Linear fits for the STC data are calculated using MATLAB to determine catalytic site distributions.

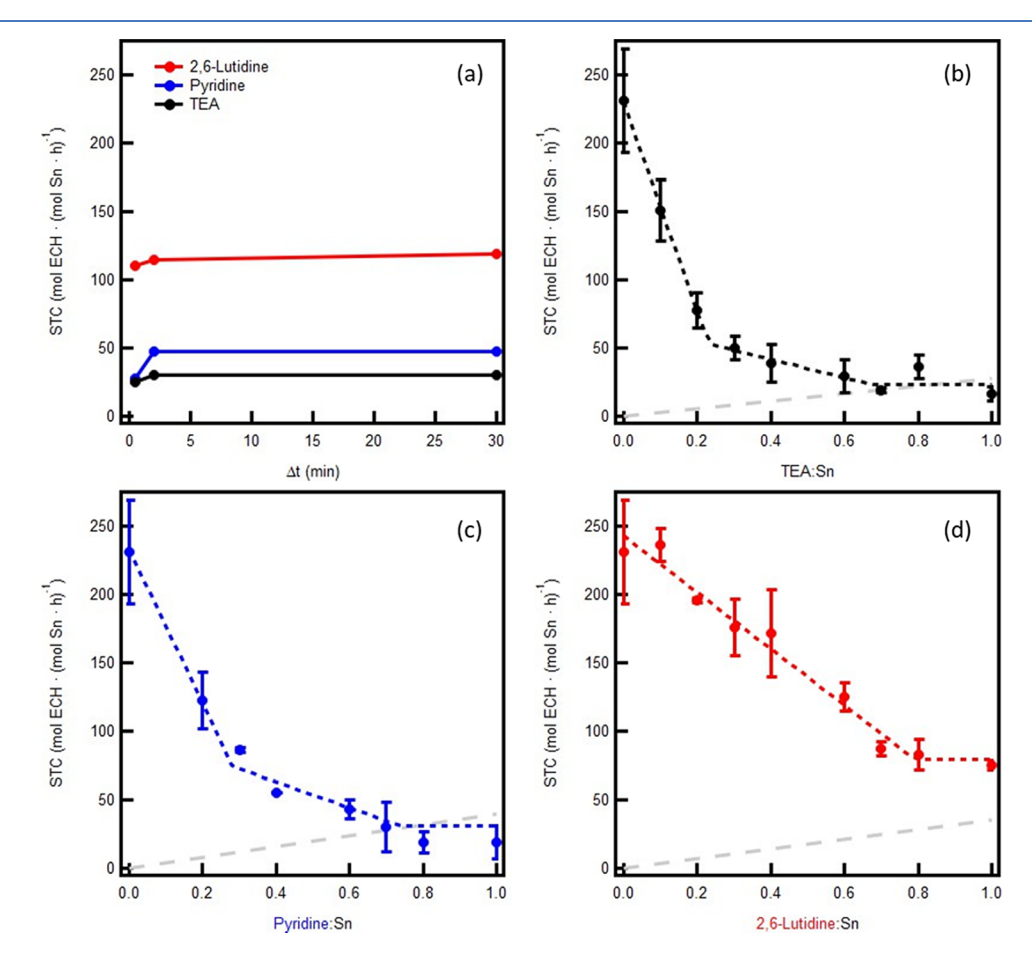


Figure 5. (a) Results of kinetic testing for diffusion limitations at a probe:Sn of 0.6. Δt refers to the amount of time for which the catalyst/probe-containing solution is stirred before beginning the reaction. Site quantification results using (b) TEA, (c) pyridine, and (d) 2,6-lutidine in hexane for Sn-Beta-200-10d. The error bars indicate one standard deviation. Dashed-colored lines are linear fits to the experimental data. Results of control experiments without catalyst are represented by dashed gray lines on each graph.

Table 2. Comparison of Catalytic Site Distributions for Sn-Beta-200-10d Determined Using Different Probes for Site Quantification Experiments

probe	% high-activity sites	% low-activity sites	total % active sites	% nonactive sites
TEA	23 ± 2	44 ± 22	67 ± 24	33 ± 24
pyridine	28 ± 4	46 ± 13	74 ± 17	26 ± 17
2,6-lutidine			82 ± 8	18 ± 8

3.3.1. Test for the Impact of Diffusion on Probe Molecules. The site quantification procedure is investigated to determine if diffusion of the probe molecule impacts the catalytic measurement by using different values of Δt —the time from when the probe-containing solution is stirred with the catalyst to when the reaction mixture is added ($\Delta t = 0.5, 2, 30$ min). These tests are conducted at a constant probe:Sn of 0.6:1. It is expected that for nondiffusion-limited poisoning, the activity would not change with Δt , whereas a diffusion-limited probe would exhibit some difference in activity.

The results of these tests are shown in Figure 5a. Results using each probe-containing solution exhibit an increase in activity from $\Delta t=0.5$ min to $\Delta t=2$ min, indicating that at 0.5 min of stirring, changes are still occurring within the system. The molecular origins of these observations are not yet evident, but it appears that a Δt of 0.5 min is not sufficient. From $\Delta t=2$ min to $\Delta t=30$ min, the activity remains the same, indicating that the probe molecules are not diffusion-limited in this time range. Therefore, it is concluded that $\Delta t=2$ min is sufficient for site quantification experiments with these probe-containing solutions.

3.3.2. Triethylamine. The results of site quantification experiments using TEA at increasing loadings are shown in Figure 5b. The initial STC at 0:1 TEA:Sn is similar to that of a standard kinetic test; the slight decrease in activity is likely because of the decreased concentration of methanol upon the addition of the probe-containing solution to the reaction mixture. From 0:1 to 0.2:1 TEA:Sn, STC decreases sharply and linearly. A decrease in activity is expected, as the Lewis basic TEA should adsorb to the Lewis acid Sn sites, rendering them inactive for the reaction. From 0.2:1 to 0.7:1 TEA:Sn, STC continues to decrease but with a distinct and less steep slope than observed for the low TEA:Sn region. This multi-slope decrease in STC indicates that TEA binds to sites that are highly active for the reaction before binding to low-activity sites; if the titration was random, the decrease in STC would instead be represented by a single slope.

Beyond 0.7:1 TEA:Sn, the activity levels off, suggesting that all of the active sites in the material have been deactivated. The STC levels off before reaching 0 mol ECH·(mol Sn·h) $^{-1}$, possibly because the probes themselves may promote ERO, which can also be catalyzed by Lewis bases.⁷² To assess the participation of TEA in the reaction, a control experiment is conducted with a reaction mixture in the absence of Sn-Beta but with the quantity of TEA that corresponds to a TEA:Sn value of 1:1. The activity of the control reaction is represented in Figure 5b by a dashed, gray, horizontal line. The control test demonstrates higher activity than the leveled-off segment of the tests with a titrated catalyst; we expect that this is because in the site quantification tests, most of the TEA is adsorbed to the catalytic sites and does not participate in the reaction, whereas in the control test, all of the added TEA is available to catalyze the reaction.

Linear fits are performed for the data using MATLAB, as we have done previously, 65 with MATLAB determining the

quantity of linear regimes as well as the slopes and ranges of each linear regime to best fit through all data points. From the MATLAB fits, the catalytic site distribution in Sn-Beta-200-10d using TEA is 23 \pm 2% high activity, 44 \pm 22% low activity, and the remainder are nonactive. The catalytic site distributions are observed using different probes on Sn-Beta-200-10d are shown in Table 2. Additionally, the MATLAB program is used to calculate the activity levels of the different types of sites. Using TEA, the high-activity sites and low-activity sites are determined to have STC values of 765 \pm 78 mol ECH·(mol Sn·h) $^{-1}$ and 67 \pm 60 mol ECH·(mol Sn·h) $^{-1}$, respectively. The difference in STC is approximately an order of magnitude.

3.3.3. Pyridine. In addition to TEA, previous work³³ has used pyridine as an active site probe, prompting us to consider this option. Following the same procedure with pyridine dosed in hexane, the site quantification experiment results (Figure 5c) are similar to those produced by TEA. The STC for 0:1 pyridine:Sn is the same as that for 0:1 TEA:Sn since the experiment does not involve the addition of probe molecules but does include a small amount of hexane. With the addition of pyridine, it is observed that STC decreases at a high rate and then at a low rate, as is the case for TEA. This indicates that pyridine is able to distinguish between sites of different activity levels in a similar manner. Finally, the control experiment adding only pyridine and no Sn-Beta—yielded similar results, with the site quantification test activity leveling off below the control test activity. Using the same MATLAB model, the site quantification experiments using pyridine indicate that Sn-Beta-200-10d has 28 \pm 4% high-activity sites and 46 \pm 13% low-activity sites. The STC values for the different sites are calculated to be 562 ± 83 mol ECH·(mol Sn·h)⁻¹ for highactivity sites and 94 \pm 30 mol ECH·(mol Sn·h)⁻¹ for lowactivity sites. The difference in STC values between TEA and pyridine for high-activity sites is attributed to the small difference in the mean fraction of high-activity sites. Overall, these results are in reasonable agreement with the results obtained using TEA.

3.3.4. 2,6-Lutidine. The site quantification results using 2,6-lutidine are unique compared to the results of TEA and pyridine; the decrease in STC follows a single slope (Figure 5d). It is likely that the methyl groups of 2,6-lutidine cause the amine to be sterically hindered, limiting the adsorption of 2,6-lutidine to the catalytic sites. This observation is consistent with previous literature in which it is concluded that 2,6-lutidine does experience steric hindrance that prevents it from distinguishing, or even adsorbing to, some Lewis acid sites. ^{71,73,74}

Additionally, 2,6-lutidine experiments result in an unexpectedly high STC at 2,6-lutidine:Sn > 0.8:1 as compared to the control test; this discrepancy may be explained by 2,6-lutidine being unable to titrate a fraction of the Lewis acid sites, a hypothesis that is supported by the appearance of a 2,6-lutidine peak in the GC-FID chromatogram (Figure S7). It is verified that peaks for pyridine and TEA are not observed in the

previous tests. These data are further discussed in SI Section S.3.3. Based on these results, 2,6-lutidine does not appear to be a good probe molecule for site quantification of Sn-Beta materials, as it is unable to distinguish between types of catalytic sites and does not appear to fully deactivate the catalytic sites to achieve an STC at or below that of the control experiment.

Overall, it is found that TEA and pyridine both provide results that distinguish between types of sites, whereas 2,6-lutidine is unable to do so. Moving forward, pyridine is used as the probe to study the effect of crystallization time on the catalytic site distribution in Sn-Beta materials, as ¹⁵N-labeled pyridine is readily available and will allow for connection to NMR experiments.

3.4. Effect of Crystallization Time—Site Quantification Experiments on Sn-Beta-200-40d. Previous studies report that Sn-Beta crystallization time impacts the catalytic site distribution and thus the activity of the material for a given reaction. Specifically, for MPVO, Sn-Beta activity increases to a maximum at 13 days and then decreases to a value lower than observed for shorter crystallization time. 10 These changes are correlated to the amounts of high-activity sites in Sn-Beta at different crystallization times. A similar trend is observed here for ERO, as Sn-Beta-200-10d has a higher activity for ERO than Sn-Beta-200-40d; this is expected because the highactivity sites for MPVO and ERO are thought to be the same. To correlate the change in activity for ERO to the catalytic site distribution, site quantification experiments are conducted using pyridine for Sn-Beta-200-40d and compared to results for Sn-Beta-200-10d.

Pyridine is tested for diffusion limitations through Sn-Beta-200-40d using a consistent methodology. Activity for ERO between epichlorohydrin and methanol does not appear to change between Δt values of 2 and 30 min, indicating that the solution is not diffusion-limited at the standard Δt value of 2 min (Figure S8). Results using pyridine on Sn-Beta-200-40d again show preferential binding to high-activity sites followed by low-activity sites (Figure 6). Sn-Beta-200-40d is found to have 19 \pm 4% high-activity sites and 60 \pm 17% low-activity sites (Table 3).

The differences in catalytic site distributions can be used to understand the trends in catalytic activity over Sn-Beta crystallization time. Sn-Beta-200-40d has less high-activity and more low-activity sites compared to Sn-Beta-200-10d, explaining Sn-Beta-200-40d's inferior performance for ERO. Although site quantification experiments appear to explain the trends in activity for ERO over crystallization time, it has yet to be seen how spectroscopic techniques connect to this narrative.

3.5. ¹⁵N MAS NMR on Sn-Beta Materials Using ¹⁵N-Labeled Pyridine. The preferential titration that is observed in site quantification experiment results may occur by (a) pyridine binding exclusively to a single type of Sn site, as previously reported, ³³ or (b) pyridine binding to both open and closed Sn sites followed by another kind of site. The order in which site binding occurs using pyridine in hexane is determined using ¹⁵N MAS NMR CP experiments after dosing ¹⁵N-labeled pyridine to Sn-Beta-200-40d at pyridine:Sn ratios of 0.15:1, 0.3:1, and 0.6:1. Based on previous literature, it is proposed that peaks near 264 and 259 ppm (referenced to ammonium chloride) are associated with pyridine binding to Sn sites and a peak near 206 ppm is assigned to the formation of pyridinium ions at SnOH groups. ⁶² Furthermore, the

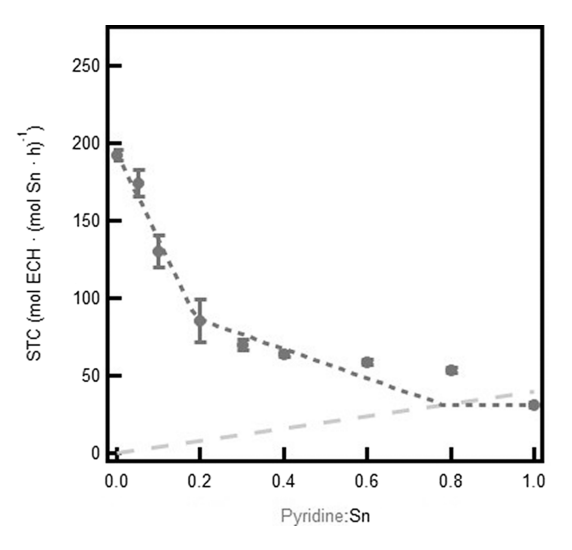


Figure 6. Site quantification experiment results and linear fits using pyridine in hexane on Sn-Beta-200-40d. The dashed dark gray lines are linear fits to the experimental data. Results of control experiments without zeolite catalysts are represented by the dashed light gray line.

chemical shift is correlated with Lewis acid strength; as Lewis acid strength of the Sn site increases, the chemical shift decreases. Therefore, the peak at 264 ppm has been assigned to pyridine binding to closed Sn sites, whereas the peak at 259 ppm is assigned to pyridine at open defect sites.

At a low pyridine:Sn of 0.15:1, peaks are observed at 264 and 259 ppm with no peak at 206 ppm (Figure 7), providing evidence for the titration of both open and closed sites but no pyridinium ion formation. At a pyridine:Sn of 0:3:1, an additional peak at 206 ppm emerges, indicating the formation of pyridinium ions at SnOH groups. Finally, at a pyridine: Sn of 0.6:1, the peak associated with closed Sn sites increases in intensity, suggesting continued binding to closed Sn sites. Thus, the following sequence is proposed: (1) pyridine adsorbs to both open defect and closed Sn sites and then (2) pyridine continues to bind to closed Sn sites, but also forms pyridinium ions at SnOH groups. These groups may be located at open defect or hydrolyzed-open Sn sites. As the ¹⁵N NMR experiments are performed via cross-polarization with ¹H nuclei, the measurements cannot be used for the quantitative determination of the fraction of sites titrated at each pyridine:Sn. For the analysis conditions, direct polarization experiments do not produce a signal for the ¹⁵N-labeled pyridine-dosed materials.

The ¹⁵N NMR experiments do enable the identification of the sites that contribute to the high-activity and low-activity regimes in the site quantification experiments (solvent phase titrations in hexane at ambient temperature followed by solvent phase reactions in methanol at 60 °C). The steep slope at low pyridine loadings represents the loss of activity from both open defect and closed sites. This observation is distinct from previous work that suggests site quantification experiments can differentiate open defect and closed Sn sites. The shallow slope at intermediate pyridine:Sn seems to be associated with the deactivation of not only closed Sn sites, but also SnOH sites, which have previously been overlooked as having their own catalytic capability for ERO, but have been considered for other reactions. ^{29,37,75} These results may help reconcile previous reports that suggest preferential site binding of pyridine to either open defect sites (titrations in vacuum at 150

Table 3. Comparison of Catalytic Site Distributions for Sn-Beta-200-10d and Sn-Beta-200-40d Determined Using Site Quantification Experiments with Pyridine in Hexane

sample	% high-activity	% low-activity	total % active	% nonactive
Sn-Beta-200-10d	28 ± 4	46 ± 13	74 ± 17	26 ± 17
Sn-Beta-200-40d	19 ± 4	60 ± 17	79 ± 21	21 ± 21

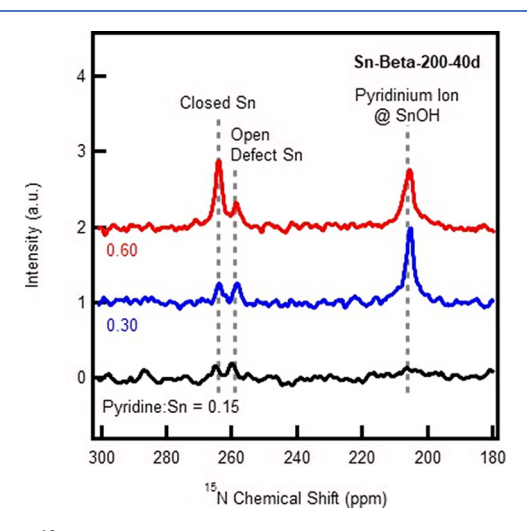


Figure 7. ¹⁵N CP-MAS NMR analysis on Sn-Beta-200-40d. Peaks at 264, 259, and 206 ppm are believed to correspond to closed Sn sites, open defect Sn sites, and pyridinium ions formed at SnOH groups, respectively.

 $^{\circ}$ C followed by solvent phase reactions in water at 100 $^{\circ}$ C) 28 or closed sites (simultaneous gas phase titration and reaction in a mixture of ethanol and water at 131 $^{\circ}$ C).

Revisiting the investigation of the effect of crystallization time on Sn-Beta structure and activity, ¹⁵N NMR results provide evidence that as crystallization time increases, the fraction of high-activity Sn sites is reduced, lowering ERO activity. Additionally, as crystallization time increases, the fraction of low-activity species (representing both SnOH and closed Sn sites) increases. The combination of ¹⁵N NMR with site quantification experiments has allowed for the establishment of a new Sn-Beta synthesis—structure—activity relationship for ERO. These results will guide future work as we aim to tune Sn-Beta to improve its activity for this valuable reaction.

4. SUMMARY

Results from site quantification experiments and spectroscopic characterization are combined to investigate the structure—activity relationships for Sn-Beta. This work identifies the use of site quantification experiments, particularly with pyridine dosed in hexane, as a promising technique for the catalytic site quantification of Sn-Beta for ERO between ECH and methanol. Pyridine appears to be nondiffusion-limited at a mixing time of 2 min. Pyridine preferentially adsorbs to high-activity sites followed by low-activity sites. TEA in hexane is also acceptable, but 2,6-lutidine in hexane is not ideal since it does not adsorb fully on the tin sites.

¹⁵N NMR provides further support for pyridine/hexane site quantification experiments. Data from ¹⁵N NMR with ¹⁵N-labeled pyridine at different loadings suggest that pyridine first binds to both open defect and closed Sn sites, followed bySnOH sites and additional closed Sn sites. These results offer new insights for the interpretation of site quantification

data, as previous studies associated the different activity losses in titration experiments to open defect vs closed Sn sites.

Overall, site quantification experiments using pyridine/hexane solutions are used to establish a new synthesis—structure—activity relationship for ERO using Sn-Beta materials: increasing crystallization times reduces the fraction of high-activity Sn sites, thereby decreasing the overall activity for the reaction between ECH and methanol. This methodology will advance our understanding of zeolites as heterogeneous catalysts and enhance their tunability to improve a wide array of industrially relevant reactions.

ASSOCIATED CONTENT

Supporting Information

The Supporting Information is available free of charge at https://pubs.acs.org/doi/10.1021/acscatal.3c02618.

Experimental details of catalyst synthesis and characterization, results of catalyst characterization, detailed results of site quantification experiments, and discussion of some site quantification results (PDF)

AUTHOR INFORMATION

Corresponding Author

Nicholas A. Brunelli — William G. Lowrie Department of Chemical and Biomolecular Engineering, The Ohio State University, Columbus, Ohio 43210, United States;
orcid.org/0000-0003-0712-8966; Email: brunelli.2@osu.edu

Authors

Leah Ford — William G. Lowrie Department of Chemical and Biomolecular Engineering, The Ohio State University, Columbus, Ohio 43210, United States

Alexander Spanos – William G. Lowrie Department of Chemical and Biomolecular Engineering, The Ohio State University, Columbus, Ohio 43210, United States

Complete contact information is available at: https://pubs.acs.org/10.1021/acscatal.3c02618

Notes

The authors declare no competing financial interest.

ACKNOWLEDGMENTS

This work was supported by the National Science Foundation (NSF Career 1653587) and SACHEM, Inc. for providing the structure-directing agent tetraethylammonium hydroxide.

REFERENCES

- (1) Chang, C.-C.; Wang, Z.; Dornath, P.; Je Cho, H.; Fan, W. Rapid Synthesis of Sn-Beta for the Isomerization of Cellulosic Sugars. *RSC Adv.* **2012**, *2*, 10475.
- (2) Kots, P. A.; Zabilska, A. V.; Khramov, E. V.; Grigoriev, Y. V.; Zubavichus, Y. V.; Ivanova, I. I. Mechanism of Zr Incorporation in the Course of Hydrothermal Synthesis of Zeolite BEA. *Inorg. Chem.* **2018**, *57*, 11978–11985.

- (3) Botti, L.; Kondrat, S. A.; Navar, R.; Padovan, D.; Martinez-Espin, J. S.; Meier, S.; Hammond, C. Solvent-Activated Hafnium-Containing Zeolites Enable Selective and Continuous Glucose—Fructose Isomerisation. *Angew. Chem., Int. Ed.* **2020**, *59*, 20017–20023.
- (4) Bermejo-Deval, R.; Assary, R. S.; Nikolla, E.; Moliner, M.; Román-Leshkov, Y.; Hwang, S. J.; Palsdottir, A.; Silverman, D.; Lobo, R. F.; Curtiss, L. A.; Davis, M. E. Metalloenzyme-like Catalyzed Isomerizations of Sugars by Lewis Acid Zeolites. *Proc. Natl. Acad. Sci. U. S. A.* **2012**, *109*, 9727–9732.
- (5) Nikolla, E.; Rodríguez, R.; Moliner, M.; Davis, M. E. "One-Pot" Synthesis of 5-(Hydroxymethyl)Furfural from Carbohydrates Using Tin-Beta Zeolite. *ACS Catal.* **2011**, *1*, 408–410.
- (6) Moliner, M.; Román-Leshkov, Y.; Davis, M. E. Tin-Containing Zeolites Are Highly Active Catalysts for the Isomerization of Glucose in Water. *Proc. Natl. Acad. Sci. U. S. A.* **2010**, *107*, 6164–6168.
- (7) Zhu, P.; Li, H.; Riisager, A. Sn-Beta Catalyzed Transformations of Sugars—Advances in Catalyst and Applications. *Catalysts* **2022**, *12*, 405.
- (8) Corma, A.; Domine, M. E.; Nemeth, L.; Valencia, S. Al-Free Sn-Beta Zeolite as a Catalyst for the Selective Reduction of Carbonyl Compounds (Meerwein-Ponndorf-Verley Reaction). *J. Am. Chem. Soc.* **2002**, *124*, 3194–3195.
- (9) Hammond, C.; Padovan, D.; Al-Nayili, A.; Wells, P. P.; Gibson, E. K.; Dimitratos, N. Identification of Active and Spectator Sn Sites in Sn- β Following Solid-State Stannation, and Consequences for Lewis Acid Catalysis. *ChemCatChem* **2015**, *7*, 3322–3331.
- (10) Kolyagin, Y. G.; Yakimov, A. V.; Tolborg, S.; Vennestrøm, P. N. R.; Ivanova, I. I. Tuning of Sn-BEA Reactivity by Controlling Tin Location in the BEA Framework. *J. Phys. Chem. C* **2021**, *125*, 26679—26687.
- (11) Corma, A.; Nemeth, L. T.; Renz, M.; Valencia, S. Sn-Zeolite Beta as a Heterogeneous Chemoselective Catalyst for Baeyer-Villiger Oxidations. *Nature* **2001**, *412*, 423–425.
- (12) Otomo, R.; Kosugi, R.; Kamiya, Y.; Tatsumi, T.; Yokoi, T. Modification of Sn-Beta Zeolite: Characterization of Acidic/Basic Properties and Catalytic Performance in Baeyer-Villiger Oxidation. *Catal. Sci. Technol.* **2016**, *6*, 2787–2795.
- (13) Meng, Q.; Liu, J.; Xiong, G.; Liu, X.; Liu, L.; Guo, H. Aerosol-Seed-Assisted Hydrothermal Synthesis of Sn-Beta Zeolite and Its Catalytic Performance in Baeyer–Villiger Oxidation. *Microporous Mesoporous Mater.* **2018**, 266, 242–251.
- (14) Kang, Z.; Zhang, X.; Liu, H.; Qiu, J.; Yeung, K. L. A Rapid Synthesis Route for Sn-Beta Zeolites by Steam-Assisted Conversion and Their Catalytic Performance in Baeyer-Villiger Oxidation. *Chem. Eng. J.* 2013, 218, 425–432.
- (15) Bare, S. R.; Kelly, S. D.; Sinkler, W.; Low, J. J.; Modica, F. S.; Valencia, S.; Corma, A.; Nemeth, L. T. Uniform Catalytic Site in Sn-β-Zeolite Determined Using X-Ray Absorption Fine Structure. *J. Am. Chem. Soc.* **2005**, 127, 12924–12932.
- (16) Meng, Q.; Liu, J.; Xiong, G.; Liu, L.; Guo, H. Fast Hydrothermal Synthesis of Hierarchical Sn-Beta Zeolite with High Sn Content in Fluoride Media. *Microporous Mesoporous Mater.* **2020**, 294, No. 109915.
- (17) Dai, W.; Lei, Q.; Wu, G.; Guan, N.; Hunger, M.; Li, L. Spectroscopic Signature of Lewis Acidic Framework and Extraframework Sn Sites in Beta Zeolites. ACS Catal. 2020, 10, 14135–14146.
- (18) Zhu, Z.; Xu, H.; Jiang, J.; Guan, Y.; Wu, P. Sn-Beta Zeolite Hydrothermally Synthesized via Interzeolite Transformation as Efficient Lewis Acid Catalyst. *J. Catal.* **2017**, 352, 1–12.
- (19) Deshpande, N.; Parulkar, A.; Joshi, R.; Diep, B.; Kulkarni, A.; Brunelli, N. A. Epoxide Ring Opening with Alcohols Using Heterogeneous Lewis Acid Catalysts: Regioselectivity and Mechanism. *J. Catal.* **2019**, *370*, 46–54.
- (20) Parulkar, A.; Spanos, A. P.; Deshpande, N.; Brunelli, N. A. Synthesis and Catalytic Testing of Lewis Acidic Nano Zeolite Beta for Epoxide Ring Opening with Alcohols. *Appl. Catal., A* **2019**, *577*, 28–34.
- (21) Tang, B.; Dai, W.; Wu, G.; Guan, N.; Li, L.; Hunger, M. Improved Postsynthesis Strategy to Sn-Beta Zeolites as Lewis Acid

- Catalysts for the Ring-Opening Hydration of Epoxides. ACS Catal. 2014, 4, 2801–2810.
- (22) Dai, W.; Wang, C.; Tang, B.; Wu, G.; Guan, N.; Xie, Z.; Hunger, M.; Li, L. Lewis Acid Catalysis Confined in Zeolite Cages as a Strategy for Sustainable Heterogeneous Hydration of Epoxides. *ACS Catal.* **2016**, *6*, 2955–2964.
- (23) Van De Vyver, S.; Odermatt, C.; Romero, K.; Prasomsri, T.; Román-Leshkov, Y. Solid Lewis Acids Catalyze the Carbon-Carbon Coupling between Carbohydrates and Formaldehyde. *ACS Catal.* **2015**, *5*, 972–977.
- (24) Su, M.; Li, W.; Zhang, T.; Xin, H. S.; Li, S.; Fan, W.; Ma, L. Production of Liquid Fuel Intermediates from Furfural via Aldol Condensation over Lewis Acid Zeolite Catalysts. *Catal. Sci. Technol.* **2017**, *7*, 3555–3561.
- (25) Lewis, J. D.; Van De Vyver, S.; Román-Leshkov, Y. Acid-Base Pairs in Lewis Acidic Zeolites Promote Direct Aldol Reactions by Soft Enolization. *Angew. Chem., Int. Ed.* **2015**, *54*, 9835–9838.
- (26) Bates, J. S.; Gounder, R. Influence of Confining Environment Polarity on Ethanol Dehydration Catalysis by Lewis Acid Zeolites. *J. Catal.* **2018**, 365, 213–226.
- (27) Wolf, P.; Liao, W. C.; Ong, T. C.; Valla, M.; Harris, J. W.; Gounder, R.; van der Graaff, W. N. P.; Pidko, E. A.; Hensen, E. J. M.; Ferrini, P.; Dijkmans, J.; Sels, B.; Hermans, I.; Copéret, C. Identifying Sn Site Heterogeneities Prevalent Among Sn-Beta Zeolites. *Helv. Chim. Acta* 2016, 99, 916–927.
- (28) Harris, J. W.; Cordon, M. J.; Di Iorio, J. R.; Vega-Vila, J. C.; Ribeiro, F. H.; Gounder, R. Titration and Quantification of Open and Closed Lewis Acid Sites in Sn-Beta Zeolites That Catalyze Glucose Isomerization. *J. Catal.* **2016**, *335*, 141–154.
- (29) Bermejo-Deval, R.; Orazov, M.; Gounder, R.; Hwang, S. J.; Davis, M. E. Active Sites in Sn-Beta for Glucose Isomerization to Fructose and Epimerization to Mannose. *ACS Catal.* **2014**, *4*, 2288–2297
- (30) Vega-Vila, J. C.; Harris, J. W.; Gounder, R. Controlled Insertion of Tin Atoms into Zeolite Framework Vacancies and Consequences for Glucose Isomerization Catalysis. *J. Catal.* **2016**, 344, 108–120.
- (31) Rai, N.; Caratzoulas, S.; Vlachos, D. G. Role of Silanol Group in Sn-Beta Zeolite for Glucose Isomerization and Epimerization Reactions. *ACS Catal.* **2013**, *3*, 2294–2298.
- (32) Hwang, S. J.; Gounder, R.; Bhawe, Y.; Orazov, M.; Bermejo-Deval, R.; Davis, M. E. Solid State NMR Characterization of Sn-Beta Zeolites That Catalyze Glucose Isomerization and Epimerization. *Top. Catal.* **2015**, *58*, 435–440.
- (33) Bates, J. S.; Bukowski, B. C.; Harris, J. W.; Greeley, J. P.; Gounder, R. Distinct Catalytic Reactivity of Sn Substituted in Framework Locations and at Defect Grain Boundaries in Sn-Zeolites. *ACS Catal.* **2019**, *9*, 6146–6168.
- (34) Boronat, M.; Corma, A.; Renz, M. Mechanism of the Meerwein Ponndorf Verley Oppenauer (MPVO) Redox Equilibrium on Snand Zr Beta Zeolite Catalysts. *J. Phys. Chem. B* **2006**, *110*, 21168—21174.
- (35) Rodríguez-Fernández, A.; Di Iorio, J. R.; Paris, C.; Boronat, M.; Corma, A.; Román-Leshkov, Y.; Moliner, M. Selective Active Site Placement in Lewis Acid Zeolites and Implications for Catalysis of Oxygenated Compounds. *Chem. Sci.* **2020**, *11*, 10225–10235.
- (36) Boronat, M.; Concepción, P.; Corma, A.; Renz, M.; Valencia, S. Determination of the Catalytically Active Oxidation Lewis Acid Sites in Sn-Beta Zeolites, and Their Optimisation by the Combination of Theoretical and Experimental Studies. *J. Catal.* **2005**, 234, 111–118.
- (37) Bukowski, B. C.; Bates, J. S.; Gounder, R.; Greeley, J. First Principles, Microkinetic, and Experimental Analysis of Lewis Acid Site Speciation during Ethanol Dehydration on Sn-Beta Zeolites. *J. Catal.* **2018**, 365, 261–276.
- (38) Lewis, J. D.; Ha, M.; Luo, H.; Faucher, A.; Michaelis, V. K.; Román-Leshkov, Y. Distinguishing Active Site Identity in Sn-Beta Zeolites Using 31P MAS NMR of Adsorbed Trimethylphosphine Oxide. ACS Catal. 2018, 8, 3076–3086.

- (39) Van De Vyver, S.; Román-Leshkov, Y. Metalloenzyme-Like Zeolites as Lewis Acid Catalysts for C-C Bond Formation. *Angew. Chem., Int. Ed.* **2015**, *54*, 12554–12561.
- (40) Wolf, P.; Valla, M.; Rossini, A. J.; Comas-Vives, A.; Núñez-Zarur, F.; Malaman, B.; Lesage, A.; Emsley, L.; Copéret, C.; Hermans, I. NMR Signatures of the Active Sites in Sn-β Zeolite. *Angew. Chem., Int. Ed.* **2014**, *53*, 10179–10183.
- (41) Osmundsen, C. M.; Spangsberg Holm, M.; Dahl, S.; Taarning, E. Tin-Containing Silicates: Structure-Activity Relations. *Proc. R. Soc. A* **2012**, *468*, 2000–2016.
- (42) Boronat, M.; Concepción, P.; Corma, A.; Renz, M. Peculiarities of Sn-Beta and Potential Industrial Applications. *Catal. Today* **2007**, 121. 39–44.
- (43) Spanos, A. P.; Parulkar, A.; Brunelli, N. A. Enhancing Hydrophobicity and Catalytic Activity of Nano-Sn-Beta for Alcohol Ring Opening of Epoxides through Post-Synthetic Treatment with Fluoride. *J. Catal.* **2021**, *404*, 430–439.
- (44) Pelmenschikov, A. G.; Van Santen, R. A.; Jänchen, J.; Meijer, E. CD3CN as a Probe of Lewis and Bronsted Acidity of Zeolites. *J. Phys. Chem.* **1993**, *97*, 11071–11074.
- (45) Chen, J.; Thomas, J. M.; Sankar, G. IR Spectroscopic Study of CD3CN Adsorbed on ALPO-18 Molecular Sieve and the Solid Acid Catalysts SAPO-18 and MeAPO-18. *J. Chem. Soc., Faraday Trans.* **1994**, *90*, 3455–3459.
- (46) Jänchen, J.; Vorbeck, G.; Stach, H.; Parlitz, B.; van Hooff, J. H. Adsorption Calorimetric and Spectroscopic Studies on Isomorphous Substituted (Al, Fe, In, Ti) MFI Zeolites. *Stud. Surf. Sci. Catal.* **1995**, 94, 108–115.
- (47) Wichterlová, B.; Tvarůžková, Z.; Sobalík, Z.; Sarv, P. Determination and Properties of Acid Sites in H-Ferrierite: A Comparison of Ferrierite and MFI Structures. *Microporous Mesoporous Mater.* 1998, 24, 223–233.
- (48) Roy, S.; Bakhmutsky, K.; Mahmoud, E.; Lobo, R. F.; Gorte, R. J. Probing Lewis Acid Sites in Sn-Beta Zeolite. *ACS Catal.* **2013**, *3*, 573–580.
- (49) Kolyagin, Y. G.; Yakimov, A. V.; Tolborg, S.; Vennestrøm, P. N. R.; Ivanova, I. I. Direct Observation of Tin in Different T-Sites of Sn-BEA by One- and Two-Dimensional 119Sn MAS NMR Spectroscopy. *J. Phys. Chem. Lett.* **2018**, *9*, 3738–3743.
- (50) Yakimov, A. V.; Kolyagin, Y. G.; Tolborg, S.; Vennestrøm, P. N. R.; Ivanova, I. I. 119Sn MAS NMR Study of the Interaction of Probe Molecules with Sn-BEA: The Origin of Penta- and Hexacoordinated Tin Formation. *J. Phys. Chem. C* 2016, 120, 28083–28092.
- (51) Wolf, P.; Valla, M.; Núñez-Zarur, F.; Comas-Vives, A.; Rossini, A. J.; Firth, C.; Kallas, H.; Lesage, A.; Emsley, L.; Copéret, C.; Hermans, I. Correlating Synthetic Methods, Morphology, Atomic-Level Structure, and Catalytic Activity of Sn- β Catalysts. *ACS Catal.* **2016**, *6*, 4047–4063.
- (52) Bermejo-Deval, R.; Gounder, R.; Davis, M. E. Framework and Extraframework Tin Sites in Zeolite Beta React Glucose Differently. *ACS Catal.* **2012**, *2*, 2705–2713.
- (53) Kolyagin, Y. G.; Yakimov, A. V.; Tolborg, S.; Vennestrøm, P. N. R.; Ivanova, I. I. Application of 119Sn CPMG MAS NMR for Fast Characterization of Sn Sites in Zeolites with Natural 119Sn Isotope Abundance. *J. Phys. Chem. Lett.* **2016**, *7*, 1249–1253.
- (54) Yakimov, A. V.; Kolyagin, Y. G.; Tolborg, S.; Vennestrøm, P. N. R.; Ivanova, I. I. Accelerated Synthesis of Sn-BEA in Fluoride Media: Effect of H2O Content in the Gel. *New J. Chem.* **2016**, *40*, 4367–4374.
- (55) Zheng, A.; Liu, S.-B.; Deng, F. 31 P NMR Chemical Shifts of Phosphorus Probes as Reliable and Practical Acidity Scales for Solid and Liquid Catalysts. *Chem. Rev.* 2017, 117, 12475.
- (56) Rakiewicz, E. F.; Peters, A. W.; Wormsbecher, R. F.; Sutovich, K. J.; Mueller, K. T. Characterization of Acid Sites in Zeolitic and Other Inorganic Systems Using Solid-State 31P NMR of the Probe Molecule Trimethylphosphine Oxide. *J. Phys. Chem. B* **1998**, *102*, 2890–2896.
- (57) Yi, X.; Ko, H. H.; Deng, F.; Liu, S.; Bin; Zheng, A. Solid-State 31P NMR Mapping of Active Centers and Relevant Spatial

- Correlations in Solid Acid Catalysts. Nat. Protoc. 2020, 15, 3527-3555.
- (58) Yang, W.; Wang, Z.; Huang, J.; Jiang, Y. Qualitative and Quantitative Analysis of Acid Properties for Solid Acids by Solid-State Nuclear Magnetic Resonance Spectroscopy. *J. Phys. Chem. C* **2021**, 125, 10179.
- (59) Johnson, B. A.; Di Iorio, J. R.; Román-Leshkov, Y. Tailoring Distinct Reactive Environments in Lewis Acid Zeolites for Liquid Phase Catalysis. *Acc. Mater. Res.* **2021**, *2*, 1033–1046.
- (60) Bornes, C.; Fischer, M.; Amelse, J. A.; Geraldes, C. F. G. C.; Rocha, J.; Mafra, L. What Is Being Measured with P-Bearing NMR Probe Molecules Adsorbed on Zeolites? *J. Am. Chem. Soc.* **2021**, *143*, 13616–13623.
- (61) Chu, Y.; Yu, Z.; Zheng, A.; Fang, H.; Zhang, H.; Huang, S. J.; Liu, S.-B.; Deng, F. Acidic Strengths of Brønsted and Lewis Acid Sites in Solid Acids Scaled by 31P NMR Chemical Shifts of Adsorbed Trimethylphosphine. *J. Phys. Chem. C* **2011**, *115*, 7660–7667.
- (62) Gunther, W. R.; Michaelis, V. K.; Griffin, R. G.; Roman-Leshkov, Y. Interrogating the Lewis Acidity of Metal Sites in Beta Zeolites with 15N Pyridine Adsorption Coupled with MAS NMR Spectroscopy. *J. Phys. Chem. C* **2016**, *120*, 28533–28544.
- (63) Chen, J.-Y.; Pineault, H.; Brunelli, N. A. Quantifying the Fraction and Activity of Catalytic Sites at Different Surface Densities of Aminosilanes in SBA-15 for the Aldol Reaction and Condensation. *J. Catal.* **2022**, *413*, 1048–1055.
- (64) Deshpande, N.; Chen, J.-Y.; Kobayashi, T.; Cho, E. H.; Pineault, H.; Lin, L.-C.; Brunelli, N. A. Investigating the Impact of Micropore Volume of Aminosilica Functionalized SBA-15 on Catalytic Activity for Amine-Catalyzed Reactions. *J. Catal.* **2022**, 414, 356–364.
- (65) Brizes, M.; Chen, J. Y.; Pineault, H.; Brunelli, N. A. Evaluating the per Site Activity of Common Mesoporous Materials as Supports for Aminosilica Catalysts for the Aldol Reaction and Condensation. *Appl. Catal.*, A 2023, 650, No. 118997.
- (66) Sushkevich, V. L.; Ivanova, I. I.; Yakimov, A. V. Revisiting Acidity of SnBEA Catalysts by Combined Application of FTIR Spectroscopy of Different Probe Molecules. *J. Phys. Chem. C* **2017**, 121, 11437–11447.
- (67) Oliviero, L.; Vimont, A.; Lavalley, J. C.; Sarria, F. R.; Gaillard, M.; Maugé, F. 2,6-Dimethylpyridine as a Probe of the Strength of Brønsted Acid Sites: Study on Zeolites. Application to Alumina. *Phys. Chem. Chem. Phys.* **2005**, *7*, 1861–1869.
- (68) Corma, A.; Rodellas, C.; Fornes, V. Characterization of Acid Surfaces by Adsorption of 2,6-Dimethylpyridine. *J. Catal.* **1984**, 88, 374–381.
- (69) Jacobs, P. A.; Heylen, C. F. Active Sites in Zeolites. III. Selective Poisoning of Bronsted Sites on Synthetic Y Zeolites. *J. Catal.* **1974**, 34, 267–274.
- (70) Morterra, C.; Cerrato, G.; Meligrana, G. Revisiting the Use of 2,6-Dimethylpyridine Adsorption as a Probe for the Acidic Properties of Metal Oxides. *Langmuir* **2001**, *17*, 7053–7060.
- (71) Nagao, M.; Misu, S.; Hirayama, J.; Otomo, R.; Kamiya, Y. Magneli-Phase Titanium Suboxide Nanocrystals as Highly Active Catalysts for Selective Acetalization of Furfural. *ACS Appl. Mater. Interfaces* **2020**, *12*, 2539–2547.
- (72) Brunelli, N. A.; Long, W.; Venkatasubbaiah, K.; Jones, C. W. Catalytic Regioselective Epoxide Ring Opening with Phenol Using Homogeneous and Supported Analogues of Dimethylaminopyridine. *Top. Catal.* **2012**, *55*, 432–438.
- (73) Benesi, H. A. Determination of Proton Acidity of Solid Catalysts by Chromatographic Adsorption of Sterically Hindered Amines. *J. Catal.* **1973**, *28*, 176–178.
- (74) Healy, M. H.; Wieserman, L. F.; Arnett, E. M.; Wefers, K. Infrared Spectroscopy and Microcalorimetric Investigations of δ - θ and K Aluminas Using Basic Probe Molecules: Acetonitrile, Pyridine, 2,6-Lutidine, and N -Butylamine. *Langmuir* **1989**, 5, 114–123.
- (75) Patet, R. E.; Fan, W.; Vlachos, D. G.; Caratzoulas, S. Tandem Diels-Alder Reaction of Dimethylfuran and Ethylene and Dehy-

dration to Para-Xylene Catalyzed by Zeotypic Lewis Acids. *ChemCatChem* **2017**, *9*, 2523–2535.

